Correlative cryogenic spectro-microscopy to investigate Selenium bioreduction products

Sirine C. Fakra[1,2*], Birgit Luef[1#], Cindy J. Castelle[1], Sean W. Mullin[1δ], Kenneth H. Williams[3], Matthew A. Marcus[2], Denise Schichnes[4], and Jillian F. Banfield[1,3]

[1]*Department of Earth and Planetary Science, University of California Berkeley, Berkeley CA 94720, USA.*

[2]*Advanced Light Source, Lawrence Berkeley National Lab, Berkeley, CA 94720, USA.*

[3]*Earth Sciences Division, Lawrence Berkeley National Lab, Berkeley, CA 94720, USA.*

[4]*Department of Plant & Microbial Biology, University of California Berkeley, Berkeley CA 94720, USA.*

[*]Corresponding author: sfakra@berkeley.edu, ph: 510-495-2855, fax: 510-486-4102.

[#]Current address: Department of Biotechnology, Norwegian University of Science and Technology, Trondheim 7491, Norway. [δ]Current address: Division of Geological and Planetary Sciences, California Institute of Technology, Pasadena, CA 91125.

Submitted to: Environmental Science and Technology.

19

Abstract

Accurate mapping of the composition and structure of minerals and associated biological materials is critical in geomicrobiology and environmental research. Here we developed an apparatus allowing correlation of cryogenic transmission electron microscopy (TEM) and synchrotron hard X-ray microprobe (SHXM) datasets to precisely determine the distribution, valence state and structure of selenium in biofilms sampled from a contaminated aquifer near Rifle, CO, USA. Results were replicated in the laboratory via anaerobic selenate-reducing enrichment cultures. 16S rRNA analyses of field-derived biofilm indicated the dominance of Betaproteobacteria from the Comamonadaceae family, and uncultivated members of the *Simplicispira* genus. The major product in field and culture-derived biofilms is ~25-300 nm red amorphous Se^0 aggregates of colloidal nanoparticles. Correlative analyses of the cultures provided direct evidence for microbial dissimilatory reduction of Se(VI) to Se(IV) to Se^0. Extended X-ray absorption fine structure spectroscopy showed red amorphous Se^0 with a first shell Se-Se interatomic distance of 2.339 ± 0.003 Å. Complementary scanning transmission X-ray microscopy revealed that these aggregates are strongly associated with a protein-rich biofilm matrix. These findings have important implications for predicting the stability and mobility of Se bioremediation products and understanding of Se biogeochemical cycling. The approach, involving correlation of cryo-SHXM and cryo-TEM datasets from the same specimen area, is broadly applicable to biological and environmental samples.

Introduction

Deciphering the roles of microbial processes in biogeochemical transformations is important for many bio-mineral systems and environmental research in general. Characterization of field samples is necessary because relevant pure cultures or characterized mixed microbial communities can be difficult to obtain, and can miss critical aspects that are key to environmental processes. Damage to biological materials can occur by shrinkage, breakage or loss of subcellular and extracellular structures. Furthermore, examination of dry or freeze-dried samples can lead to denaturation of proteins, alteration of the mineral structure and loss of spatial resolution at the cell surface-nanoparticle interface, yielding incorrect interpretations[1].

Most bio-mineral samples are complex, of variable chemical composition at the nano- and micro-scales, and often contain poorly-ordered materials in low concentration. Synchrotron hard X-ray microprobes (SHXM) are ideally suited to characterize such systems, and provide metal distribution through X-ray fluorescence mapping (μXRF), valence state, local atomic structure via X-ray absorption spectroscopy (μXAS) and phase by X-ray diffraction (μXRD)[2]. X-ray damage through metal photo-reduction/oxidation and amorphization has been well documented and is especially acute in organics-containing samples[3-5] . Selenium (Se) compounds in particular are prone to X-ray damage as illustrated by the breaking of the Cγ—Se bond in selenomethionine (SeMet)[6], selenate photoreduction[7] and selenite photo-oxidation[8] or just simply reported such as in the case of Se-contaminated biological wastewater samples[9]. Additionally, organic-bound metals and low-Z containing molecules are often difficult to analyze at room temperature because thermal vibrations damp the amplitude of extended X-ray absorption fine structure (EXAFS) oscillations, especially at high photo-electron wavenumbers. These issues are exacerbated in dilute and/or poorly ordered bio-minerals where longer beam exposure is usually

63 required for adequate signal-to-noise ratios. To alleviate these effects, measurements are most
64 often carried out at LN_2 (77 K) or less frequently at LHe (4 K) temperatures. In the case of
65 selenium, prior Se K-edge cryo-EXAFS studies of amorphous and crystalline Se[10] demonstrated
66 that the Debye-Waller thermal disorder component is only marginally reduced below 100 K,
67 suggesting that the use of LHe (versus LN_2) would not significantly improve the EXAFS signal.
68 Lastly, cryogenic analyses should allow better detection of any potentially volatile selenides
69 produced.

70 There is a strong incentive to link cryogenic SHXM with cryogenic transmission electron
71 microscopy (cryo-TEM[11]). Cryo-TEM provides ultra-structural information at 2-4 nm
72 resolution[12]. Whole frozen hydrated intact bacteria embedded in amorphous (vitreous) ice can be
73 analyzed, eliminating artifacts associated with traditional fixation and dehydration methods or
74 sectioning[1]. The sample is generally cooled with LN_2 (vs. LHe[13]), and low dose imaging mode is
75 used to minimize electron damage and preserve sample structures in a "near-native" state.
76 However, cryo-TEM provides limited chemical information on thin samples ($\lesssim$ 750 nm) within a
77 narrow field of view (100's nm). On the other hand, SHXM is effective at characterizing, at the
78 micron scale, millimeter-scale areas of poorly concentrated samples (10's of ppm). Ultimately
79 correlating cryo-TEM with cryo-SHXM datasets of the same sample region allows to link sub-
80 nm-scale structural information to crucial chemical speciation data. Here we use this approach to
81 investigate the distribution and speciation of selenium in biofilms from an unconfined aquifer
82 adjacent to the Colorado River, near Rifle, CO, USA. The shallow groundwater has residual
83 metal contamination (U, V, As and Se) at tens of μM levels due to past ore-milling activities.
84 These levels exceed U.S. E.P.A. drinking water standards (100 nM for Se). To date, the potential

for acetate amendments into the subsurface to stimulate uranium bioreduction has been extensively studied[14-17] whereas microbiological and geochemical processes controlling selenium mobility, thus toxicity at the site and others similar, are poorly understood.

Se occurs predominantly in four oxidation states (VI, IV, 0 and –II). Se oxyanions, selenate (Se(VI), SeO_4^{2-}) and selenite (Se(IV), SeO_3^{2-}), are toxic at ppm concentrations and known to bioaccumulate in the food chain causing significant ecological damage[18]. The biogeochemical cycle of Se in nature is not well defined[19] but is predominantly governed by microorganisms[20]. An important part of this cycle is the dissimilatory[21] reduction of Se oxyanions (DSeR) by anaerobes[22]. These microorganisms couple the oxidation of organic matter (or H_2) to the reduction of Se oxyanions, forming either relatively insoluble non-toxic Se^0 or reactive and toxic selenide Se(-II). Dissimilatory selenate reduction to Se^0 is a major sink for Se oxyanions in anoxic environments[22, 23]. Although phylogenetically diverse selenite-reducing bacteria have been well characterized, relatively little is known about selenate-reducing bacteria. On the other hand, the stability, reactivity and bioavailability of Se^0 colloids are still not well understood, and likely depend strongly on the size, morphology and allotropic form of Se. A handful of studies have reported microbial reduction of Se oxyanions to Se^0, mostly as red amorphous[24-28] (primarily chain structure) and red crystalline monoclinic[29] (Se_8 rings). However, few provide direct evidence of the structure of the Se allotropes produced, especially from field-preserved samples.

Previously at the Rifle site, microbial reduction of Se oxyanions was detected during a biostimulation experiment[30], but many questions remained about the form(s) and distribution of the products. Here we developed a cryo-stage that allows the transfer of cryogenically preserved

Se-rich biofilms between a TEM and a SHXM, enabling essentially artifact-free ultra-structural biological and chemical information from the same sample region. We used this approach to examine in detail the spatial distribution and chemical speciation of selenium in samples obtained through field experimentation at the Rifle site and cultivation.

Materials and Methods

Additional materials and methods can be found in the Supporting Information.

Biofilm samples from the Rifle site. The samples were collected during the "Super 8" uranium bio-stimulation field experiment[17] (August-September 2010) at the Rifle Integrated Field Research Challenge site adjacent to the Colorado River (Western Colorado, USA). The site is located on a relatively low-lying alluvial terrace created by a floodplain meander of the Colorado River and is described extensively elsewhere[14, 16]. The shallow, unconfined aquifer consists of alluvial sands, silts, and gravels; details on the geochemistry and mineralogy can be found in prior studies[15, 16]. As previously described[17], the groundwater was amended with sodium acetate and injected into the subsurface at various depths. Acetate (CH_3COO^-) served as a carbon source and electron donor over the course of the 25-day amendment period. Biofilm samples were collected at well CG02 (4 m depth, 5 mM acetate), close to the down-gradient reference well CD01, 16 days after injection of acetate to the anoxic aquifer. For all analyses except confocal laser scanning microscopy, samples were collected by scraping the biofilm off the injection tubing (polyethylene, HDPE) used to circulate the acetate-amended groundwater (pH~7.2). The biofilms were uniformly distributed across the tubing, with minimal O_2 (from

diffusion across the tubing wall) and low nitrate level (~10 μM average). Samples were flash-frozen directly in the field, to preserve their physical and chemical integrity, using a portable cryo-plunger[31] and procedures described in the Supporting Information.

Enrichment cultures. For enrichment cultivation, we sampled pieces of the tubing used to deliver acetate to the subsurface, in which a biofilm had grown onto the inner surface and preserved these pieces at -80 °C. Some pieces of biofilm were used for PCR amplification of 16S rRNA gene sequencing (see details in Supporting Information). Other pieces of biofilm were thawed and added anaerobically to fresh medium in a glove box. Cultures were established either in 10 mL carbonate-buffered freshwater medium (sulfate and nitrate free) or in groundwater artificial medium (GWA, contains sulfate) and inoculated with sodium selenate or sodium selenite (5 mM, Sigma Aldrich) and sodium acetate or sodium L- lactate (10 mM, Sigma Aldrich). Details regarding the growth media can be found in the Supporting Information (Table S1). Cultures were sparged with N_2:CO_2 (80:20) to remove dissolved oxygen and sealed with butyl rubber stoppers and aluminum crimp seals, as previously described[32]. All cultures were incubated at room temperature in the dark. Only cultures grown anaerobically using acetate as the carbon source and electron donor and selenate as the sole electron acceptor were further analyzed. Red precipitates were observed after 5 days, suggesting selenate reduction to Se^0. Samples were flash-frozen in the lab at various time points then stored in LN_2 until analyses.

2D cryo-TEM Cryo-TEM images were acquired with a JEOL–3100-FFC electron microscope (JEOL Ltd, Akishima, Tokyo, Japan) equipped with a FEG electron source operating at 300 kV, an Omega energy filter (JEOL), an LN_2-cooled sample transfer stage (80 K), and a Gatan 795 4K×4K CCD camera (Gatan Inc., Pleasanton, CA, USA) mounted at the exit of an

electron decelerator held at a voltage of 200 to 250 kV. Survey of the grids and selection of suitable targets were performed in low dose defocused diffraction mode. Images were recorded at different magnifications with a pixel size of 0.56 and 0.701 nm at the specimen. Several images were recorded with a 2K×2K CCD camera instead, with a pixel size of 0.69, 0.92 and 1.2 nm at the specimen. Underfocus values ranged from 12± 0.5 µm to 15± 0.5 µm, and energy filter widths were typically around 30 eV. Over 100 images of field samples and 70 images of culture samples were recorded to evaluate the morphology and size of cells and colloidal particles.

X-ray microprobe. Micro-focused X-ray fluorescence (µXRF) mapping, X-ray diffraction (µXRD) and Se K-edge X-ray absorption spectroscopy data were collected at the Advanced Light Source (ALS) bending magnet beamline 10.3.2 (2.4- 17 keV) with the storage ring operating at 500 mA and 1.9 GeV[33]. All data were recorded at 95 K using a cryo-stage described below. Maps and µXRF spectra were collected at 13 keV with a beam spot size ranging from 2×2 µm to 5×5 µm, and counting times up to 200 ms/pixel. Fluorescence emission counts were recorded using a seven-element Ge solid-state detector (Canberra) and XIA electronics. Se K-edge µXANES spectra were recorded in fluorescence mode by continuously scanning the Si (111) monochromator (Quick XAS mode) from 160 eV below up to 407 eV above the edge (12500-13067 eV, i.e. up to k = 10 $Å^{-1}$). EXAFS spectra were recorded up to 740 eV above the edge (12500-13400 eV, i.e. up to k ~ 13.7 $Å^{-1}$). Spectra were calibrated using the white line of a red amorphous Se standard set at 12660 eV. All data were processed using LabVIEW custom software and standard procedures described elsewhere[34]. To rapidly survey the valence state of selenium in the samples, valence state scatter plots were generated from XANES data using a spectral database of Se compounds (see **Table S2** and Supporting

Information). Further, least-squares linear combination fitting of the XANES spectra was performed as previously described[35]. Micro-EXAFS spectra of cultures were reduced with $k^2\chi(k)$ weighting, out to k = 12 Å^{-1} and analyzed via shell-by-shell fitting using the FEFF6l code and the Artemis software[36, 37]. Only the first shell was fitted, as other shells were not visible enough for accurate analysis. The structure of trigonal Se^0 as described by Keller and coworkers[38] was used to create FEFF6l input files from which to extract Se-Se paths out to 3.5 Å and fit the experimental *t*-Se EXAFS spectrum at 95 K. Fit of the culture data were performed in q space (2-12 Å) using a Kaiser-Bessel window (1.4-2.5 Å). Details on μXRD analyses can be found in the Supporting Information.

Correlative cryogenic SHXM and TEM. A custom X-ray microprobe cryo-stage (-190 to +150 °C, ±0.1°C precision) was designed and built in collaboration with Instec Inc, to fit the geometry of the beamline and allow cryo-transfer of flash-frozen samples (**Figures 1** and **S1**). The apparatus allows cryo-XRF/XAS measurements to be performed in fluorescence and/or transmission modes. XRD measurements in transmission, are used to check for ice contamination and quality of the transfer. The apparatus consists of four parts: a stage (CLM77K), a sample loading frame (SLF) that can accommodate two round sample grid boxes, a grid holder tongue (GHT) and a temperature controller (mk1000). Prior to any cold experiment, the CLM77K stage is heated to +110°C for 5 minutes then purged with dry N_2 gas to remove any moisture trapped. The CLM77K is cooled to -190 °C (83 K) using a pressurized LN_2 tank. During cooling, the sample chamber and all windows are purged with dry N_2 gas to prevent water vapor condensation and frost. The SLF, placed in a LN_2 bath in a Styrofoam container, is used to support the GHT during sample loading/unloading. Using the SLF, a single cryo-TEM

grid (or Si_3N_4 window), mounted in a JEOL 3100 TEM cartridge, can be loaded onto the GHT for correlative analyses. Alternatively, another GHT designed to accommodate up to three TEM grids (or windows) can also be used. In either configuration, the spring loaded GHT cover snaps closed over the cryo-TEM grids, keeping them thermally insulated. Once the CLM77K is cooled and stable at -190 ± 0.1°C, the GHT containing the cryo-samples, is then quickly inserted and locked into the CLM77K, where the sample temperature reaches 95 K. Thermocouples located in the GHT and CLM77K, and connected to the mk1000 are used to continuously monitor (every second) the temperature of the sample and the stage respectively. Once the cryo-microprobe measurements (~12 h maximum duration) are complete, the GHT with samples is cryo-transferred back to the SLF in an LN_2 bath and samples are subsequently stored in LN_2.

Results and discussion

Geochemistry

Biofilm samples (referred as 'biofilm CG02') were collected 16 days after the start of acetate amendment in the subsurface, during the Fe(III) reduction period[39]. Acetate injection into the aquifer resulted in a rapid decrease of soluble Se; the minimum concentration was reached after 7 days (**Figure S2**). The concentration of dissolved Se (Se oxyanions) just prior to acetate injection on day 1 was 0.81 μM, versus 0.03 μM on day 15 (closest time point to sample collection), suggesting that ~96% of dissolved Se was converted into a solid phase. Soluble Se concentration remained well below the U.S. EPA limit for Se in drinking water (0.1μM) past biostimulation experiment. Sulfate concentrations remained stable indicating minimal sulfate reduction and sulfide production during the sampling period. These trends are consistent with

prior acetate biostimulation experiments[16] on un-amended portions of the Rifle aquifer as was the case here.

Microbial community composition

Phylogenetic analyses of the 16S rRNA gene sequences recovered from biofilm CG02 show an abundance of organisms from the Betaproteobacteria class (72% of the community sequences, **Figures S3 and S4**). These bacteria are often found dominant in freshwaters and inferred to play an important role in the nitrogen cycle, including nitrate respiration. Comamonadaceae is the most abundant family **(Figure S3C)** and uncultivated members of the *Simplicispira* genus were the most abundant identified organisms (**Figures S3D and S4B**). It is well known from prior studies at this site that acetate enriches for members of the Comamonadaceae family, specifically the *Simplicispira*[40] genus. In fact, this result was shown previously in well CD01, the same groundwater reference well used in the current study[41]. The facultative anaerobe *Simplicispira* strain BDI[42] (motile, weakly-curved rod) a nitrate and vanadate reducer, was isolated from this site. We tested this isolate for selenate or selenite reduction to Se^0. The organism was cultivated both in nitrate-free and nitrate-amended (2 mM) bicarbonate freshwater medium inoculated with acetate (5, 10 mM) and selenate (5 mM) or selenite (1, 2 and 5 mM). No red (or grey/black/brown) Se^0 precipitates were formed, indicating that strain BDI does not carry out this transformation in solutions containing mM concentrations of these Se oxyanions. A large number of uncultivated members of the Comamonadaceae family were detected, some of which could contribute to the reduction of Se oxyanions. However, we could not test this hypothesis because to date only the BDI strain has been isolated from this site. Some members of the Comamonadaceae family such as *Comamonas sp.* are known selenite

238 reducers[43]. Identified genus from this family, *Hydrogenophaga sp.* (H_2-oxidizer) are rod-shaped,
239 autotrophic denitrifiers[44] that have been correlated with nitrate and selenate fluxes[45]. These
240 organisms likely contribute to selenate reduction because some strains have been reported to
241 reduce selenate and selenite to dimethyl selenide (DMSe) and dimethyl diselenide (DMDSe) [46].

242 The second most abundant family detected was Rhodocyclaceae (**Figures S3C and**
243 **S4C**), which contains many denitrifying bacteria. Among identified genera from this family, rod-
244 shaped *Zoogloea sp.* (9%), contains strains capable of denitrification[47] and of selenite reduction
245 to elemental Se[48]. *Zoogloea sp.* have also been previously detected in Se-rich biofilms from
246 Rifle[30]. *Ferribacterium sp*.[49] and *Dechloromonas* RCB form a monophyletic group (**Figure S4C**)
247 representing 5% of the bacterial community. *Dechloromonas sp.* are well-known perchlorate and
248 nitrate-reducing bacteria[50] commonly found or used to enhance selenate reduction in
249 bioreactors[51, 52]. *Hydrogenophaga sp., Zoogloea sp.* and *Dechloromonas sp.* have been
250 previously detected in Se-rich biofilms[30] at Rifle and have been often detected at this site over
251 the years[30, 53-57]. Finally, bacteria from the Chloroflexi and the Bacteroidetes phyla could also
252 contribute to selenate reduction because a variety of selenate reductases have been identified in
253 the genomes of Anaerolineaceae and Bacteroidetes[58] obtained from the Rifle site
254 (http://ggkbase.berkeley.edu/). .

255 Organisms from unidentified genera and uncultivated *Simplicispira* members account for
256 nearly three-quarters of the bacterial community. Their potential role in Se oxyanions reduction
257 is unknown and warrants further investigation. These results suggest uncultivated members of
258 the Comamonadaceae family may play an important role in Se oxyanions reduction at this
259 location.

260 **Ultrastructure and carbon speciation of the field and culture samples**

261 3D confocal microscopy of biofilm CG02 revealed a 2 to 12 μm thick biofilm with
262 several haystacks of self-organized cells (**Movie S1**). On the surface of the haystack, the cells
263 range in size from 0.75 to 2.7 μm (**Movie S2**). Within the core and bottom of the stack, cells are
264 similar in length, but with an oval shape. In both field and culture samples, cells exhibited a
265 Gram-negative cell wall with an inner membrane, an outer membrane and a peptidoglycan layer
266 within a periplasmic space (**Figures 2 and S5**). Cells were weakly curved rods, rod-, oval- or
267 round-shaped, with the latter only observed in biofilm CG02. Few cells exhibited an S-layer;
268 many had visible polar flagella and/or pili. Most bacteria from biofilm CG02 had pili (**Figure**
269 **S5**). Most cells contained cytoplasmic granules. STXM-derived C K-edge XANES spectra of
270 granules (**Figure S6**) exhibits a major peak at 288.4 eV, attributed to carboxyls or esters[59, 60],
271 likely associated with polyhydroxyalkanoates (polyesters), carbon, electron and energy storage
272 polymers commonly produced by bacteria under limited nutrients. Carbon storage granules have
273 been widely reported in organisms we detected by 16S rRNA, such as *Simplicispira sp.*[40],
274 *Dechloromonas sp.*[61], *Hydrogenophaga sp.*[62] *and Zoogloea sp.*[47, 63]. Further, a prior study[64] on
275 members of the Comamonadaceae family showed that a N-poor medium tends to stimulate the
276 production of polyhydroxyalkanoates, whereas a C-poor environment leads to the production of
277 polyphosphates. Carbon K-edge STXM data on field and culture samples (**Figures S6 and S7)**
278 showed abundant Se-rich aggregates associated with a thick protein-rich biofilm matrix
279 containing extracellular polymeric substances (EPS) rich in acidic polysaccharides with a peak at
280 288.6 eV (π*(C=O) transition of carboxyl group in acidic polysaccharides) and in carbonates,

with a signature π*(C=O) peak at ~ 290.3 eV. In the cultures, Se^0 CNPs located near cell surfaces were coated with a protein-rich organic layer (**Figure S7**).

Selenium distribution and speciation in the field and culture samples

In both field and culture samples, the vast majority of colloidal nanoparticles (CNPs) were found as extracellular aggregates, or as few electron dense particles on cell surfaces. SEM imaging and energy dispersive spectroscopy of these particles (**Figure S8**) showed Se, with traces of Ca (and Si) from the background medium. The biofilm CG02 particles were about 160 nm ±70 nm in diameter while the particles in the culture grown in bicarbonate medium were a bit smaller at about 130±70 nm (**Figure S9**). Only a few Se CNPs were found on each individual cell surface as seen from TEM and STXM data. Se $L_{2,3}$ edges XANES spectra of CNPs compared to model compounds are shown in **Figure S10 .** The spectra of Se standards are consistent with prior reports[65, 66] and spectra of CNPs from field and culture samples closely match that of red amorphous Se^0. However the allotropic form of Se cannot be accurately determined at these absorption edges and thus further analysis of these spectra was not pursued.

By contrast, most Se compounds can easily be classified by K-edge XANES, due to a clear shift (2-3 eV) of the edge position ('white line') depending on Se oxidation state (**Figure 3**). This can be explained by dipole selection rules where 1s core electrons are excited into the unoccupied 4p electronic states and the edge position shifts towards higher energy as the oxidation state increases. Standard spectra are consistent with prior studies[67-70]. Twenty nine, eighteen and twenty three Se-rich regions were investigated by μXANES on biofilm CG02, cultures grown in bicarbonate or GWA medium, respectively, to get enough statistics. Cultures

were analyzed up to 60 days after the addition of selenate and acetate to the medium to determine the end products. Typical Se K-edge XANES of the CNPs from biofilm CG02 and cultures grown in bicarbonate medium are displayed in **Figure 3,** and most closely resemble that of red amorphous Se. Se valence plots and least-square linear combination fitting (LSQF) of the XANES spectra (see methods and Supporting Information) indicate red amorphous Se^0 is the major end product in all samples (**Figure 4 and Table S3**). Attempt at fitting the data with other Se^0 compounds such as red monoclinic-α Se, black amorphous Se and grey hexagonal Se did not yield good fits. These results were further confirmed by μXRD (**Figure S11**) on field and culture samples which showed no evidence for crystalline Se (either hexagonal or monoclinic). There is an accumulation of selenite during selenate reduction in the culture samples that is not observed in the field data, as evidenced both in the valence plot (**Figure 4**) and fitting results (**Table S3**).

Correlated cryogenic SHXM/ TEM analyses of a 19-day-old culture in bicarbonate medium are shown in **Figure 5 and S11**. A cluster of bacteria is found associated with ~100 ± 60 nm diameter Se^0 CNPs and traces of Se(IV). Organo-selenium and inorganic selenides were not detected in this region, suggesting that reduction proceeds in a two-step reaction from Se(VI) to Se(IV) to Se(0). Compared to a prior study on Se-rich biofilm[30], correlated cryogenic SHXM/ TEM allows identification of the forms of selenium present on intact organisms and resolution of their ultrastructure and associated minerals. Considering the low X-ray dose applied to the frozen samples (see Supporting Information), photo-reduction is an unlikely explanation for the formation of these compounds. The corresponding μXRD spectrum (**Figure S11B**) does not show a match to crystalline Se^0 (either hexagonal or monoclinic). Furthermore, we compared EXAFS spectra of Se^0 CNPs from biofilm CG02 and bicarbonate cultures (**Figure 6, Table S4)**

with the crystal structure of hexagonal Se^0, as determined by Keller et al.[38] The 1st shell (Se-Se bond) lies at 2.355 ± 0.003 Å for the biofilm CG02 and at 2.339 ± 0.003 Å for the bicarbonate culture, respectively. These inter-atomic distances are shorter than the bond length in hexagonal Se (2.374 Å) and are consistent with previous reports for amorphous Se[71,72]. Only the first shell could be fitted by a shell-by-shell method, the 2nd shell was not sufficiently visible to fit due to lack of structural order, thus the Se-Se-Se bond angle could not be determined. The coordination numbers (N) and sigma square (σ^2) values of the samples are very similar. The biofilm CG02 exhibits the longest bond length among the two samples reflecting a less disordered structure.

Although a vast majority of the data indicated red amorphous Se^0, a few regions analyzed outside thick biofilm regions in the 19-day-old culture show crystallization, as evidenced by diffraction contrast and the presence of planar defects, likely twin planes (**Figure S12**). It is interesting that crystallization occurred over just 19 days at 25 °C, given that transformation of bulk red amorphous Se to grey trigonal Se should occur at appreciable rates only above ~50 °C[73]. Nonetheless, in both cultures and field samples red amorphous Se was stable for months.

Dissimilatory and assimilatory selenate reducers

Cryo-spectromicroscopy and 16S rRNA gene sequence analysis of field and culture samples suggest the presence of DSeR organisms. In that process, selenate used as the sole terminal electron acceptor is sequentially reduced to selenite and Se^0 and further to selenide. Our cultivation conditions involved high selenate concentration and resulted in significant production of red amorphous Se (~30% of the volume). Dissimilatory reduction of selenate and selenite by anaerobic bacteria generally produces abundant extracellular Se^0 particles[29], consistent with our

observations. Selenite is a known intermediate in the microbial dissimilatory reduction of selenate, being produced and reduced concomitantly. By contrast, the assimilatory microbial reduction of selenate does not produce selenite[20] but leads to the formation of organoselenium and selenides, both found as minor components in our samples. Selenite can be dissimilatory reduced to Se^0 and further to selenide (e.g. H_2Se) or it can be assimilatory reduced to organoselenium (e.g., SeMet) and volatile selenides (e.g. DMSe)[74]

The presence of organic Se in our samples could be attributed to either cell lysis, selenate-tolerant bacteria or potentially selenite to selenide reducing bacteria. Selenate reduction is mediated by either a soluble periplasmic selenate reductase (SerABC) or a nitrate reductase or via a dissimilatory sulfate-reducing pathway. A wide variety of selenate reductases have been identified in the genomes of bacteria from the Rifle site (http://ggkbase.berkeley.edu/). Selenite is usually imported into the cytoplasm where it is reduced to Se^0 via a membrane-associated reductase, followed by rapid expulsion of Se particles via a membrane efflux pump[75]. Selenite is reduced by reacting with proteins in a "Painter-type" reaction, suggested as a general microbial detoxification reaction to Se oxyanions[76].

When using sulfate-containing media (GWA), some sulfate-reducing anaerobes could also be capable of reducing μM amounts of selenate, although they generally do not couple this reduction to growth[28, 77]. Moreover, the ability of sulfate respirers to reduce selenate (or selenite) is greatly constrained by the availability of sulfate. Se oxyanions are thermodynamically predicted to be reduced prior to sulfate[22] according to their respective redox potentials (+0.44 V for SeO_4^{2-}/SeO_3^{2-}, +0.21 V for SeO_3^{2-}/Se^0, -0.22 V for SO_4^{2-}/H_2S and -0.52 V for SO_4^{2-}/SO_3^{2-}). At the shallow depth (4 meters) where biofilms were collected, the sulfate concentration (8 mM,

367 **Figure S2**) is at a level that usually precludes selenate reduction by sulfate reducers[21, 77]. By
368 contrast, DSeR microorganisms can reduce mM amounts of selenate to Se^0, consistent with our
369 observations. In part due to similar potentials for the SeO_4^{2-}/ SeO_3^{2-} (+0.44 V) and NO_3^-/NO_2^-
370 (+0.42 V) redox couples, microbial reduction of nitrate and selenate often occur close together[78,
371 79], consistent with the presence of denitrifying bacteria we find by 16S rRNA gene sequencing
372 analyses.

373 **Accumulation of selenite in cultures**

374 The accumulation of selenite observed during growth on selenate, regardless of the
375 medium used, could occur because the microbial community reduces selenate faster than
376 selenite. Alternatively, Se oxidizers may re-oxidize Se^0 to selenite. The first hypothesis is the
377 most likely, as reduction of selenite to red Se^0 by the cultures was minimal, and occurred very
378 slowly (over weeks). Oxidation of Se^0 by Se-oxidizers cannot be ruled out considering the large
379 pool of unidentified organisms, however that process is generally very slow [80]. More importantly
380 in our cultures, cells are under different geochemical conditions than in the field and are
381 subjected to concentrations of Se oxyanions orders of magnitude higher (5 mM versus ~1 μM),
382 selectively enriching for few members of the community.

383 **Association of red amorphous Se CNPs with proteins**

384 Our results show that Se^0 CNPs are strongly associated with proteins in the biofilm[81, 82].
385 Particles may be surface stabilized from dissolution or phase transformation when embedded in
386 the protein-rich biofilm matrix, as suggested by prior research on biogenic and synthetic Se^0
387 nanoparticles in the presence of proteins[83, 84]. Previous studies have suggested the presence of

388 surface-associated proteins on Se^0 produced by selenite reducers[85]. More generally, prior studies
389 have shown that biogenic (and synthetic) selenium nanoparticles can be associated with a
390 plenitude of high-affinity proteins[83, 86]. Proteins, peptides, and amino acids could be released
391 after cell death[87] and scavenged by hydrophobic elemental selenium surfaces. Alternatively,
392 bacteria may also excrete Se-binding proteins[24]. Finally, Se^0 particles found outside cells could
393 have been released through cell lysis[28], as we have observed in old culture samples. Any of these
394 processes would lead to extracellular aggregation of Se^0 nanoparticles, preventing entombment
395 of cells. The aggregation of Se particles likely affects selenium mobility and transport[88], as
396 evidenced by prior work showing that aggregation induced by extracellular metal-binding
397 polypeptides and proteins plays an important role in constraining the dispersion of nanoparticles
398 in the environment[89].

399 Many anthropogenic activities (e.g., agriculture, petroleum refining, mining, glass and
400 pigment manufacturing) generate Se contaminated wastewaters. Existing treatment technologies,
401 based on chemical co-precipitation or adsorption, are rather inefficient, especially for selenate,
402 and too expensive for practical industrial use. Bioremediation represents an attractive alternative
403 approach, but strongly relies on determining accurately the chemical speciation and distribution
404 of the bio-reduction products in order to be directly applicable to a diversity of anaerobic soil and
405 groundwater environments contaminated with selenium.

406 The community of Se oxyanions reducers detected here includes several genera
407 previously detected in Se-rich biofilms collected under similar conditions at the Rifle site[30].
408 However, the distribution patterns and allotropic form of selenium found here are clearly
409 distinct. The prior study suggested the presence of cells encrusted with red monoclinic Se^0, but

using our novel correlative cryogenic spectro-microscopy apparatus, we demonstrate that the main product is extracellular red amorphous Se^0 captured in a protein-rich biofilm matrix and that only few particles are associated with each cell surface. Both the newly identified protein coating and extensive particle aggregation are expected to reduce re-oxidation rates, thereby minimizing the rapid re-release of aqueous Se to the environment.

Acknowledgments

This material is partially based upon work supported through the Lawrence Berkeley National Laboratory's Sustainable Systems Scientific Focus Area. The U.S. D.O.E. Office of Science, Office of Biological and Environmental Research funded the work under contracts DE-SC0004733 and DE-AC02-05CH11231. Part of the equipment was funded by the LBL EFRC Center for Nanoscale Control of Geologic CO_2. We thank Paul Baker at Instec Inc. for his help with the microprobe cryo-stage, Sue Spaulding for lab support, Tolek Tylizscack for support at ALS beamline 11.0.2, Mary Gilles and Steve Kelly for sharing their ESEM. We are grateful to D. Strawn, A. Ryser, E.A.H. Pilon-Smits and J.L. Freeman for sharing their selenium standard spectra. The Advanced Light Source is supported by the Office of Basic Energy Sciences, Office of Science, U.S. D.O.E. Contract No. DE-AC02-05CH11231.

Supporting Information

Additional experimental details, figures, and tables as referenced in the text. This material is available free of charge via the Internet at http://pubs.acs.org.

References

1. Dohnalkova, A. C.; Marshall, M. J.; Arey, B. W.; Williams, K. H.; Buck, E. C.; Fredrickson, J. K., Imaging Hydrated Microbial Extracellular Polymers: Comparative Analysis by Electron Microscopy. *Appl. Environ. Microbiol.* **2011,** *77*, (4), 1254-1262.
2. Manceau A., M. A. M., N. Tamura, *Quantitative speciation of metals in soils and sediments. Applications of synchrotron radiation* 2002; Vol. 49.
3. Howells, M. R.; Hitchcock, A. P.; Jacobsen, C. J., Introduction: Special issue on radiation damage. *J. Electron Spectrosc. Relat. Phenom.* **2009,** *170*, (1–3), 1-3.
4. Fayard, B.; Salomé, M.; Takemoto, K.; Kihara, H.; Susini, J., Some practical considerations about the effects of radiation damage on hydrated cells imaged by X-ray fluorescence microscopy. *J. Electron Spectrosc. Relat. Phenom.* **2009,** *170*, (1–3), 19-24.
5. Cody, G. D.; Brandes, J.; Jacobsen, C.; Wirick, S., Soft X-ray induced chemical modification of polysaccharides in vascular plant cell walls. *J. Electron Spectrosc. Relat. Phenom.* **2009,** *170*, (1–3), 57-64.
6. Holton, J., XANES measurements of the rate of radiation damage to selenomethionine side chains. *J. Synch. Rad.* **2007,** *14*, (1), 51-72.
7. George, G. N.; Pickering, I. J.; Pushie, M. J.; Nienaber, K.; Hackett, M. J.; Ascone, I.; Hedman, B.; Hodgson, K. O.; Aitken, J. B.; Levina, A.; Glover, C.; Lay, P. A., X-ray-induced photo-chemistry and X-ray absorption spectroscopy of biological samples. *J. Synch. Rad.* **2012,** *19*, (6), 875-886.
8. Huggins, F. E.; Sanei, H., Synchrotron-radiation-induced oxidation of selenite to selenate in coal-derived fly ash. *J. Synch. Rad.* **2011,** *18*, (3), 530-533.
9. Lenz, M.; van Hullebusch, E. D.; Farges, F.; Nikitenko, S.; Corvini, P. F. X.; Lens, P. N. L., Combined Speciation Analysis by X-ray Absorption Near-Edge Structure Spectroscopy, Ion Chromatography, and Solid-Phase Microextraction Gas Chromatography−Mass Spectrometry To Evaluate Biotreatment of Concentrated Selenium Wastewaters. *Environ. Sci. Technol.* **2010,** *45*, (3), 1067-1073.
10. Kolobov, A. V.; Oyanagi, H.; Tanaka, K.; Tanaka, K., Structural study of amorphous selenium by in situ EXAFS: Observation of photoinduced bond alternation. *Phys. Rev. B* **1997,** *55*, (2), 726-734.
11. Milne, J. L. S.; Subramaniam, S., Cryo-electron tomography of bacteria: progress, challenges and future prospects. *Nat Rev Micro* **2009,** *7*, (9), 666-675.
12. Comolli, L. R.; Banfield, J. F., Inter-species interconnections in acid mine drainage microbial communities. *Frontiers in Microbiology* **2014,** *5*, 367.
13. Comolli, L. R.; Downing, K. H., Dose tolerance at helium and nitrogen temperatures for whole cell electron tomography. *Journal of Structural Biology* **2005,** *152*, (3), 149-156.
14. Anderson, R. T.; Vrionis, H. A.; Ortiz-Bernad, I.; Resch, C. T.; Long, P. E.; Dayvault, R.; Karp, K.; Marutzky, S.; Metzler, D. R.; Peacock, A.; White, D. C.; Lowe, M.; Lovley, D. R., Stimulating the In Situ Activity of Geobacter Species To Remove Uranium from the Groundwater of a Uranium-Contaminated Aquifer. *Appl. Environ. Microbiol.* **2003,** *69*, (10), 5884-5891.

15. Campbell, K. M.; Kukkadapu, R. K.; Qafoku, N. P.; Peacock, A. D.; Lesher, E.; Williams, K. H.; Bargar, J. R.; Wilkins, M. J.; Figueroa, L.; Ranville, J.; Davis, J. A.; Long, P. E., Geochemical, mineralogical and microbiological characteristics of sediment from a naturally reduced zone in a uranium-contaminated aquifer. *Appl. Geochem.* **2012,** *27*, (8), 1499-1511.
16. Williams, K. H.; Long, P. E.; Davis, J. A.; Wilkins, M. J.; N'Guessan, A. L.; Steefel, C. I.; Yang, L.; Newcomer, D.; Spane, F. A.; Kerkhof, L. J.; McGuinness, L.; Dayvault, R.; Lovley, D. R., Acetate Availability and its Influence on Sustainable Bioremediation of Uranium-Contaminated Groundwater. *Geomicrobiol. J.* **2011,** *28*, (5-6), 519-539.
17. Bao, C.; Wu, H.; Li, L.; Newcomer, D.; Long, P. E.; Williams, K. H., Uranium Bioreduction Rates across Scales: Biogeochemical Hot Moments and Hot Spots during a Biostimulation Experiment at Rifle, Colorado. *Environ. Sci. Technol.* **2014,** *48*, (17), 10116-10127.
18. Santolo, O. H. M. a. G. M., Kesterson Reservoir-Past, Present, and Future: An Ecological Risk Assessment. In *Selenium in the Environment*, W.T. Frankenberger, J., and S.M. Benson, Ed. Marcel Dekker: 1994; pp 69-117.
19. Shrift, A., A Selenium Cycle in Nature? *Nature* **1964,** *201*, (4926), 1304-1305.
20. W.T. Frankenberger, J., and S.M. Benson, *Selenium in the environment*. Marcel Dekker, Inc. ed.; Taylor & Francis: N.Y.C., N.Y., 1994.
21. Lovley, D. R., Dissimilatory Metal Reduction. *Annu. Rev. Microbiol.* **1993,** *47*, (1), 263-290.
22. Oremland, R. S.; Hollibaugh, J. T.; Maest, A. S.; Presser, T. S.; Miller, L. G.; Culbertson, C. W., Selenate Reduction to Elemental Selenium by Anaerobic Bacteria in Sediments and Culture: Biogeochemical Significance of a Novel, Sulfate-Independent Respiration. *Appl. Environ. Microbiol.* **1989,** *55*, (9), 2333-2343.
23. Steinberg, N. A.; Oremland, R. S., Dissimilatory Selenate Reduction Potentials in a Diversity of Sediment Types. *Appl. Environ. Microbiol.* **1990,** *56*, (11), 3550-3557.
24. Debieux, C. M.; Dridge, E. J.; Mueller, C. M.; Splatt, P.; Paszkiewicz, K.; Knight, I.; Florance, H.; Love, J.; Titball, R. W.; Lewis, R. J.; Richardson, D. J.; Butler, C. S., A bacterial process for selenium nanosphere assembly. *Proc. Natl. Acad. Sci. U. S. A.* **2011,** *108*, (33), 13480-13485.
25. Hunter, W.; Manter, D., Reduction of Selenite to Elemental Red Selenium by Pseudomonas sp. Strain CA5. *Curr Microbiol* **2009,** *58*, (5), 493-498.
26. Kessi, J.; Ramuz, M.; Wehrli, E.; Spycher, M.; Bachofen, R., Reduction of Selenite and Detoxification of Elemental Selenium by the Phototrophic BacteriumRhodospirillum rubrum. *Appl. Environ. Microbiol.* **1999,** *65*, (11), 4734-4740.
27. Tomei, F. A.; Barton, L. L.; Lemanski, C. L.; Zocco, T. G., Reduction of selenate and selenite to elemental selenium by Wolinella succinogenes. *Can. J. Microbiol.* **1992,** *38*, (12), 1328-1333.
28. Tomei, F.; Barton, L.; Lemanski, C.; Zocco, T.; Fink, N.; Sillerud, L., Transformation of selenate and selenite to elemental selenium byDesulfovibrio desulfuricans. *J. Ind. Microbiol.* **1995,** *14*, (3-4), 329-336.
29. Oremland, R. S.; Herbel, M. J.; Blum, J. S.; Langley, S.; Beveridge, T. J.; Ajayan, P. M.; Sutto, T.; Ellis, A. V.; Curran, S., Structural and Spectral Features of Selenium Nanospheres Produced by Se-Respiring Bacteria. *Appl. Environ. Microbiol.* **2004,** *70*, (1), 52-60.

30. Williams, K. H.; Wilkins, M. J.; N'Guessan, A. L.; Arey, B.; Dodova, E.; Dohnalkova, A.; Holmes, D.; Lovley, D. R.; Long, P. E., Field evidence of selenium bioreduction in a uranium-contaminated aquifer. *Environ Microbiol Rep.* **2013,** *5*, (3), 444-452.
31. Comolli, L. R.; Duarte, R.; Baum, D.; Luef, B.; Downing, K. H.; Larson, D. M.; Csencsits, R.; Banfield, J. F., A portable cryo-plunger for on-site intact cryogenic microscopy sample preparation in natural environments. *Microsc Res Tech* **2012,** *75*, (6), 829-836.
32. Coates, J. D.; Phillips, E. J.; Lonergan, D. J.; Jenter, H.; Lovley, D. R., Isolation of Geobacter species from diverse sedimentary environments. *Appl. Environ. Microbiol.* **1996,** *62*, (5), 1531-6.
33. Marcus, M. A.; MacDowell, A. A.; Celestre, R.; Manceau, A.; Miller, T.; Padmore, H. A.; Sublett, R. E., Beamline 10.3.2 at ALS: a hard X-ray microprobe for environmental and materials sciences. *J. Synch. Rad.* **2004,** *11*, (3), 239-247.
34. Kelly, S. D., Hesterberg, D., & Ravel, B, Analysis of Soils and Minerals Using X-ray Absorption Spectroscopy. In *Mineralogical Methods*, Drees, A. L. U. L. R., Ed. Soil Science Society of America: Madison, WI, 2008; Vol. Part 5, p 367.
35. Bañuelos, G. S.; Fakra, S. C.; Walse, S. S.; Marcus, M. A.; Yang, S. I.; Pickering, I. J.; Pilon-Smits, E. A. H.; Freeman, J. L., Selenium Accumulation, Distribution, and Speciation in Spineless Prickly Pear Cactus: A Drought- and Salt-Tolerant, Selenium-Enriched Nutraceutical Fruit Crop for Biofortified Foods. *Plant Physiol.* **2011,** *155*, (1), 315-327.
36. Newville, M., IFEFFIT: interactive XAFS analysis and FEFF fitting. *J. Synchrotron Radiation* **2001,** *8*, (2), 322-324.
37. Ravel, B.; Newville, M., ATHENA, ARTEMIS, HEPHAESTUS: data analysis for X-ray absorption spectroscopy using IFEFFIT. *J. Synchrotron Radiation* **2005,** *12*, (4), 537-541.
38. Keller, R.; Holzapfel, W. B.; Schulz, H., Effect of pressure on the atom positions in Se and Te. *Phys. Rev. B* **1977,** *16*, (10), 4404-4412.
39. Luef, B.; Fakra, S. C.; Csencsits, R.; Wrighton, K. C.; Williams, K. H.; Wilkins, M. J.; Downing, K. H.; Long, P. E.; Comolli, L. R.; Banfield, J. F., Iron-reducing bacteria accumulate ferric oxyhydroxide nanoparticle aggregates that may support planktonic growth. *ISME J* **2013,** *7*, (2), 338-350.
40. Grabovich, M.; Gavrish, E.; Kuever, J.; Lysenko, A. M.; Podkopaeva, D.; Dubinina, G., Proposal of Giesbergeria voronezhensis gen. nov., sp. nov. and G. kuznetsovii sp. nov. and reclassification of [Aquaspirillum] anulus, [A.] sinuosum and [A.] giesbergeri as Giesbergeria anulus comb. nov., G. sinuosa comb. nov. and G. giesbergeri comb. nov., and [Aquaspirillum] metamorphum and [A.] psychrophilum as Simplicispira metamorpha gen. nov., comb. nov. and S. psychrophila comb. nov. *INT J SYST EVOL MICR* **2006,** *56*, (3), 569-576.
41. Yelton, A. P.; Williams, K. H.; Fournelle, J.; Wrighton, K. C.; Handley, K. M.; Banfield, J. F., Vanadate and Acetate Biostimulation of Contaminated Sediments Decreases Diversity, Selects for Specific Taxa, and Decreases Aqueous V5+ Concentration. *Environ. Sci. Technol.* **2013,** *47*, (12), 6500-6509.
42. Yelton, A. P. Metagenomic and Cultivation-Based Analysis of Novel Microorganisms and Functions in Metal-Contaminated Environments. UC Berkeley, Berkeley, 2012.
43. Zheng, S.; Su, J.; Wang, L.; Yao, R.; Wang, D.; Deng, Y.; Wang, R.; Wang, G.; Rensing, C., Selenite reduction by the obligate aerobic bacterium Comamonas testosteroni S44 isolated from a metal-contaminated soil. *BMC microbiology* **2014,** *14*, 204.

44. Willems, A.; Busse, J.; Goor, M.; Pot, B.; Falsen, E.; Jantzen, E.; Hoste, B.; Gillis, M.; Kersters, K.; Auling, G.; De Ley, J., Hydrogenophaga, a New Genus of Hydrogen-Oxidizing Bacteria That Includes Hydrogenophaga flava comb. nov. (Formerly Pseudomonas flava), Hydrogenophaga palleronii (Formerly Pseudomonas palleronii), Hydrogenophaga pseudoflava (Formerly Pseudomonas pseudoflava and "Pseudomonas carboxydoflava"), and Hydrogenophaga taeniospiralis (Formerly Pseudomonas taeniospiralis). *Int. J. Syst. Evol. Bac.* **1989,** *39*, (3), 319-333.
45. Lai, C.-Y.; Yang, X.; Tang, Y.; Rittmann, B. E.; Zhao, H.-P., Nitrate Shaped the Selenate-Reducing Microbial Community in a Hydrogen-Based Biofilm Reactor. *Environ. Sci. Technol.* **2014,** *48*, (6), 3395-3402.
46. Ranjard, L.; Prigent-Combaret, C.; Favre-Bonté, S.; Monnez, C.; Nazaret, S.; Cournoyer, B., Characterization of a novel selenium methyltransferase from freshwater bacteria showing strong similarities with the calicheamicin methyltransferase. *BBA - Gene Structure and Expression* **2004,** *1679*, (1), 80-85.
47. Dugan, P.; Stoner, D.; Pickrum, H., The Genus Zoogloea. In *The Prokaryotes*, Dworkin, M.; Falkow, S.; Rosenberg, E.; Schleifer, K.-H.; Stackebrandt, E., Eds. Springer New York: 2006; pp 960-970.
48. Srivastava, N.; Mukhopadhyay, M., Biosynthesis and structural characterization of selenium nanoparticles mediated by Zooglea ramigera. *Powder Technol.* **2013,** *244*, (0), 26-29.
49. Cummings, D. E.; Caccavo Jr, F.; Spring, S.; Rosenzweig, R. F., Ferribacterium limneticum, gen. nov., sp. nov., an Fe(III)-reducing microorganism isolated from mining-impacted freshwater lake sediments. *Arch Microbiol* **1999,** *171*, (3), 183-188.
50. Coates, J. D.; Chakraborty, R.; Lack, J. G.; O'Connor, S. M.; Cole, K. A.; Bender, K. S.; Achenbach, L. A., Anaerobic benzene oxidation coupled to nitrate reduction in pure culture by two strains of Dechloromonas. *Nature* **2001,** *411*, (6841), 1039-1043.
51. Zhang, Y.; Frankenberger Jr, W. T., Supplementing Bacillus sp. RS1 with Dechloromonas sp. HZ for enhancing selenate reduction in agricultural drainage water. *Sci. Total Environ.* **2007,** *372*, (2–3), 397-405.
52. Chung, J.; Ryu, H.; Abbaszadegan, M.; Rittmann, B. E., Community structure and function in a H(2)-based membrane biofilm reactor capable of bioreduction of selenate and chromate. *Appl Microbiol Biotechnol* **2006,** *72*, (6), 1330-1339.
53. Mouser, P. J.; N'Guessan, A. L.; Elifantz, H.; Holmes, D. E.; Williams, K. H.; Wilkins, M. J.; Long, P. E.; Lovley, D. R., Influence of Heterogeneous Ammonium Availability on Bacterial Community Structure and the Expression of Nitrogen Fixation and Ammonium Transporter Genes during in Situ Bioremediation of Uranium-Contaminated Groundwater. *Environ. Sci. Technol.* **2009,** *43*, (12), 4386-4392.
54. N'Guessan, A. L.; Elifantz, H.; Nevin, K. P.; Mouser, P. J.; Methe, B.; Woodard, T. L.; Manley, K.; Williams, K. H.; Wilkins, M. J.; Larsen, J. T.; Long, P. E.; Lovley, D. R., Molecular analysis of phosphate limitation in Geobacteraceae during the bioremediation of a uranium-contaminated aquifer. *ISME J* **2009,** *4*, (2), 253-266.
55. Handley, K. M.; Wrighton, K. C.; Piceno, Y. M.; Andersen, G. L.; DeSantis, T. Z.; Williams, K. H.; Wilkins, M. J.; N'Guessan, A. L.; Peacock, A.; Bargar, J.; Long, P. E.; Banfield, J. F., High-density PhyloChip profiling of stimulated aquifer microbial communities reveals a complex response to acetate amendment. *FEMS Microbiol. Ecol.* **2012,** *81*, (1), 188-204.

56. Wrighton, K. C.; Thomas, B. C.; Sharon, I.; Miller, C. S.; Castelle, C. J.; VerBerkmoes, N. C.; Wilkins, M. J.; Hettich, R. L.; Lipton, M. S.; Williams, K. H.; Long, P. E.; Banfield, J. F., Fermentation, Hydrogen, and Sulfur Metabolism in Multiple Uncultivated Bacterial Phyla. *Science* **2012,** *337*, (6102), 1661-1665.
57. Wrighton, K. C.; Castelle, C. J.; Wilkins, M. J.; Hug, L. A.; Sharon, I.; Thomas, B. C.; Handley, K. M.; Mullin, S. W.; Nicora, C. D.; Singh, A.; Lipton, M. S.; Long, P. E.; Williams, K. H.; Banfield, J. F., Metabolic interdependencies between phylogenetically novel fermenters and respiratory organisms in an unconfined aquifer. *ISME J* **2014,** *8*, (7), 1452-1463.
58. Handley, K. M.; VerBerkmoes, N. C.; Steefel, C. I.; Williams, K. H.; Sharon, I.; Miller, C. S.; Frischkorn, K. R.; Chourey, K.; Thomas, B. C.; Shah, M. B.; Long, P. E.; Hettich, R. L.; Banfield, J. F., Biostimulation induces syntrophic interactions that impact C, S and N cycling in a sediment microbial community. *ISME J* **2013,** *7*, (4), 800-816.
59. Boyce, C. K.; Cody, G. D.; Feser, M.; Jacobsen, C.; Knoll, A. H.; Wirick, S., Organic chemical differentiation within fossil plant cell walls detected with X-ray spectromicroscopy. *Geology* **2002,** *30*, (11), 1039-1042.
60. Cody, G. D.; Ade, H.; Wirick, S.; Mitchell, G. D.; Davis, A., Determination of chemical-structural changes in vitrinite accompanying luminescence alteration using C-NEXAFS analysis. *Organic Geochem.* **1998,** *28*, (7–8), 441-455.
61. Salinero, K.; Keller, K.; Feil, W.; Feil, H.; Trong, S.; Di Bartolo, G.; Lapidus, A., Metabolic analysis of the soil microbe Dechloromonas aromatica str. RCB: indications of a surprisingly complex life-style and cryptic anaerobic pathways for aromatic degradation. *BMC Genomics* **2009,** *10*, (1), 351.
62. Yoon, S. C.; Choi, M. H., Local Sequence Dependence of Polyhydroxyalkanoic Acid Degradation in Hydrogenophaga pseudoflava. *J. Biol. Chem.* **1999,** *274*, (53), 37800-37808.
63. Saito, T.; Saegusa, H.; Miyata, Y.; Fukui, T., Intracellular degradation of poly(3-hydroxybutyrate) granules of Zoogloea ramigera I-16-M. *FEMS Microbiol. Lett.* **1992,** *103*, (2-4), 333-338.
64. Spring, S.; Wagner, M.; Schumann, P.; Kämpfer, P., Malikia granosa gen. nov., sp. nov., a novel polyhydroxyalkanoate- and polyphosphate-accumulating bacterium isolated from activated sludge, and reclassification of Pseudomonas spinosa as Malikia spinosa comb. nov. *Int. J Syst Evol Micr.* **2005,** *55*, (2), 621-629.
65. J. Madwid, R. A., R. Blyth, I. Coulthard, C.J. Doonan, D. Liu, R. Hoffmeyer, M.J. Pushie, T. Regier, J. Ruszkowski, S.P. Singh, D. Thavarajah, C.I.E. Wiramanaden, S.I. Yang, L. Zhang, G.N. George, I.J. Pickering *Selenium L-edge spectroscopy at the SGM Beamline as a tool for environmental selenium speciation*; CLS: 2008.
66. Bugaris, D. E.; Copping, R.; Tyliszczak, T.; Shuh, D. K.; Ibers, J. A., La2U2Se9: An Ordered Lanthanide/Actinide Chalcogenide with a Novel Structure Type. *Inorg. Chem.* **2010,** *49*, (5), 2568-2575.
67. Pickering, I. J.; Brown, G. E.; Tokunaga, T. K., Quantitative Speciation of Selenium in Soils Using X-ray Absorption Spectroscopy. *Environmental Science & Technology* **1995,** *29*, (9), 2456-2459.
68. Ryser, A.; Strawn, D.; Marcus, M.; Johnson-Maynard, J.; Gunter, M.; Moller, G., Micro-spectroscopic investigation of selenium-bearing minerals from the Western US Phosphate Resource Area. *Geochemical Transactions* **2005,** *6*, (1), 1.

69. Ryser, A. L.; Strawn, D. G.; Marcus, M. A.; Fakra, S.; Johnson-Maynard, J. L.; Möller, G., Microscopically Focused Synchrotron X-ray Investigation of Selenium Speciation in Soils Developing on Reclaimed Mine Lands. *Environmental Science & Technology* **2005,** *40*, (2), 462-467.
70. Sarret, G.; Avoscan, L.; Carrière, M.; Collins, R.; Geoffroy, N.; Carrot, F.; Covès, J.; Gouget, B., Chemical Forms of Selenium in the Metal-Resistant Bacterium Ralstonia metallidurans CH34 Exposed to Selenite and Selenate. *Applied and Environmental Microbiology* **2005,** *71*, (5), 2331-2337.
71. Majid, M.; Bénazeth, S.; Souleau, C.; Purans, J., XAFS study of interchain and intrachain order in Se1-xTex glasses: Nearest neighbors. *Phys. Rev. B* **1998,** *58*, (10), 6104-6114.
72. Yang, S. I.; Lawrence, J. R.; Swerhone, G. D. W.; Pickering, I. J., Biotransformation of selenium and arsenic in multi-species biofilm. *Environ. Chem.* **2011,** *8*, (6), 543-551.
73. Minaev, V. S.; Timoshenkov, S. P.; Kalugin, V. V., Structural and phase transformations in condensed selenium. *J Optoelectron Adv Mater.* **2005,** *7*, (4), 1717-1741.
74. Herbel, M. J.; Blum, J. S.; Oremland, R. S.; Borglin, S. E., Reduction of Elemental Selenium to Selenide: Experiments with Anoxic Sediments and Bacteria that Respire Se-Oxyanions. *Geomicrobiol. J.* **2003,** *20*, (6), 587-602.
75. Losi, M. E.; Frankenberger, W. T., Reduction of Selenium Oxyanions by Enterobacter cloacae SLD1a-1: Isolation and Growth of the Bacterium and Its Expulsion of Selenium Particles. *Appl. Environ. Microbiol.* **1997,** *63*, (8), 3079-84.
76. Harrison, J. J.; Ceri, H.; Turner, R. J., Multimetal resistance and tolerance in microbial biofilms. *Nat Rev Micro* **2007,** *5*, (12), 928-938.
77. Zehr, J. P.; Oremland, R. S., Reduction of Selenate to Selenide by Sulfate-Respiring Bacteria: Experiments with Cell Suspensions and Estuarine Sediments. *Appl. Environ. Microbiol.* **1987,** *53*, (6), 1365-1369.
78. Oremland, R. S.; Blum, J. S.; Bindi, A. B.; Dowdle, P. R.; Herbel, M.; Stolz, J. F., Simultaneous Reduction of Nitrate and Selenate by Cell Suspensions of Selenium-Respiring Bacteria. *Appl. Environ. Microbiol.* **1999,** *65*, (10), 4385-4392.
79. Steinberg, N. A.; Blum, J. S.; Hochstein, L.; Oremland, R. S., Nitrate Is a Preferred Electron Acceptor for Growth of Freshwater Selenate-Respiring Bacteria. *Appl. Environ. Microbiol.* **1992,** *58*, (1), 426-428.
80. Dowdle, P. R.; Oremland, R. S., Microbial Oxidation of Elemental Selenium in Soil Slurries and Bacterial Cultures. *Environ. Sci. Technol.* **1998,** *32*, (23), 3749-3755.
81. Flemming, H. C.; Wingender, J., The biofilm matrix. *Nature reviews. Microbiology* **2010,** *8*, (9), 623-33.
82. Sutherland, I. W., The biofilm matrix – an immobilized but dynamic microbial environment. *Trends in Microbiol.* **2001,** *9*, (5), 222-227.
83. Dobias, J.; Suvorova, E. I.; Bernier-Latmani, R., Role of proteins in controlling selenium nanoparticle size. *Nanotechnology* **2011,** *22*, (19), 195605.
84. Kaur, G.; Iqbal, M.; Bakshi, M. S., Biomineralization of Fine Selenium Crystalline Rods and Amorphous Spheres. *J Phys Chem C* **2009,** *113*, (31), 13670-13676.
85. Pearce, C. I.; Pattrick, R. A. D.; Law, N.; Charnock, J. M.; Coker, V. S.; Fellowes, J. W.; Oremland, R. S.; Lloyd, J. R., Investigating different mechanisms for biogenic selenite transformations: Geobacter sulfurreducens, Shewanella oneidensis and Veillonella atypica. *Env. Technol.* **2009,** *30*, (12), 1313-1326.

86. Lenz, M.; Kolvenbach, B.; Gygax, B.; Moes, S.; Corvini, P. F., Shedding light on selenium biomineralization: proteins associated with bionanominerals. *Appl Environ Microbiol* **2011,** *77*, (13), 4676-80.
87. Bayles, K. W., The biological role of death and lysis in biofilm development. *Nat Rev Micro* **2007,** *5*, (9), 721-726.
88. Buchs, B.; Evangelou, M. W. H.; Winkel, L. H. E.; Lenz, M., Colloidal Properties of Nanoparticular Biogenic Selenium Govern Environmental Fate and Bioremediation Effectiveness. *Environ. Sci. Technol.* **2013,** *47*, (5), 2401-2407.
89. Moreau, J. W.; Weber, P. K.; Martin, M. C.; Gilbert, B.; Hutcheon, I. D.; Banfield, J. F., Extracellular Proteins Limit the Dispersal of Biogenic Nanoparticles. *Science* **2007,** *316*, (5831), 1600-1603.

706

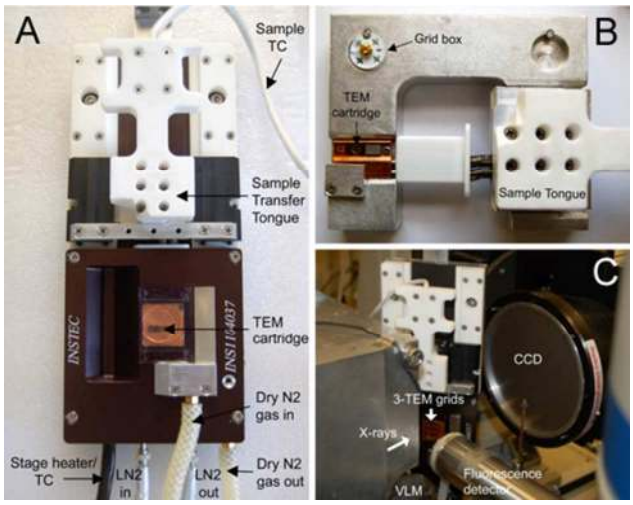

Figure 1. SHXM cryo-stage allowing correlative cryogenic TEM/microprobe measurements. A) CLM77K stage with the JEOL 3100 TEM cartridge sample transfer tongue inserted. B) View of the cartridge grid holder tongue installed on the mounting frame. C) View of the stage at beamline 10.3.2, with the sample transfer tongue inserted. The sample is oriented at 45 degrees to the incident beam, micro-XRD is performed in transmission mode.

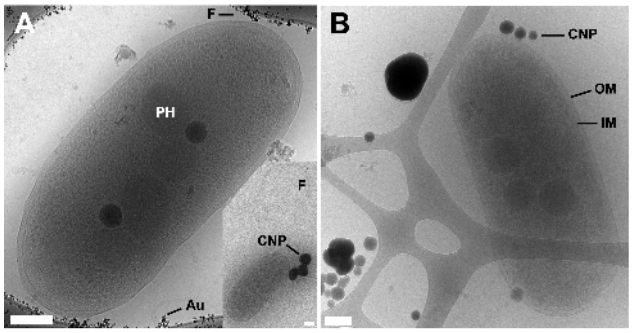

Figure 2. Cryo-TEM images of anaerobes, colloidal nanoparticles and aggregates from (A) Biofilm CG02 and (B) Selenate-reducing enrichment culture (19-day-old) grown in bicarbonate medium. IM = inner membrane, OM= outer membrane, F= flagellum, PH= polyhydroxyalkanoates, CNP= colloidal nanoparticles, Au= gold fiducial particles on a carbon coated lacey Formvar film. Scale bars are 200 nm.

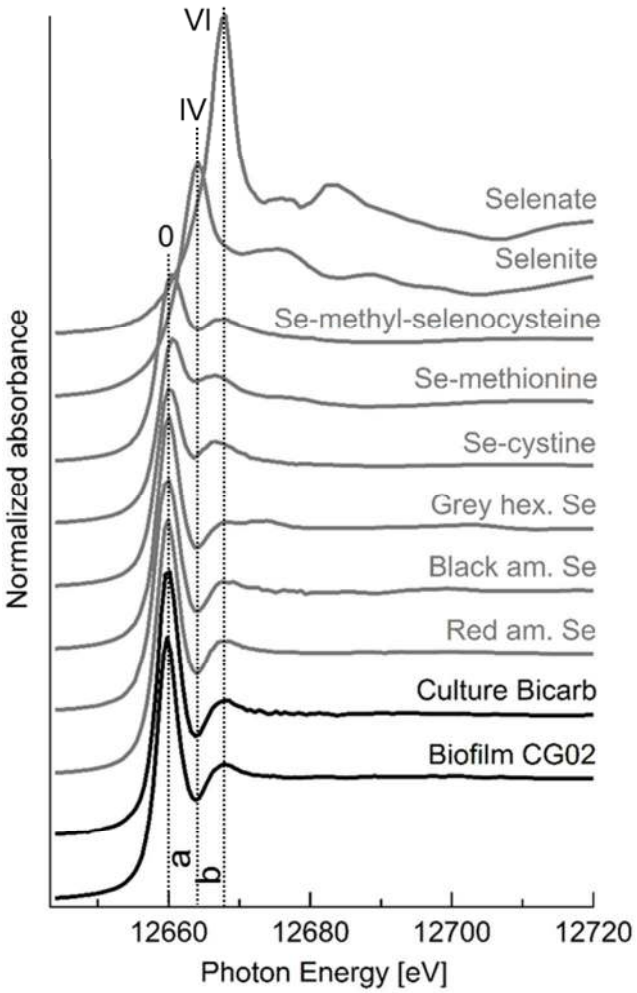

Figure 3. Se K-edge μXANES spectra of biofilm CG02 and of a 19-day-old culture grown in bicarbonate medium, compared with a subset of standards (see **Table S2** for the complete list). Normalized XANES values at 12664.25 (IV dashed line) and 12667.8 eV (VI dashed line) were used to generate the Se valence state plot displayed in **Figure 4** (see Supporting Information).

707

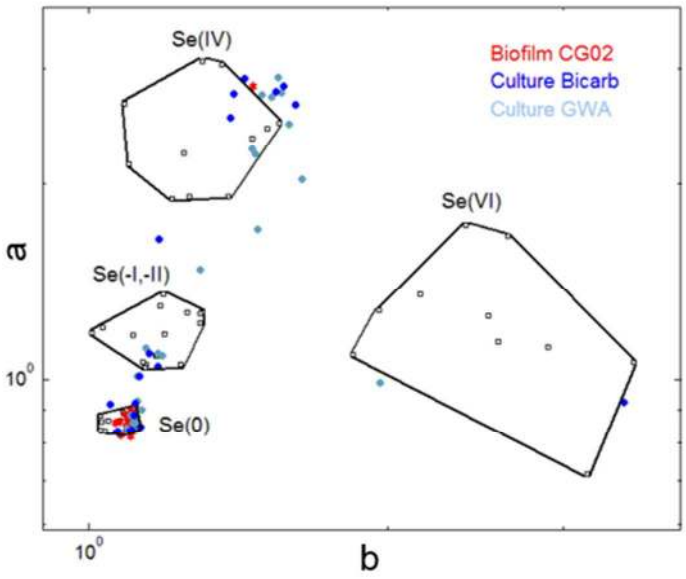

Figure 4. Se valence state scatter plot. The standards are shown in open black squares, the biofilm CG02 in red (29 spots) and the enrichment cultures grown in bicarbonate medium in dark blue (18 spots) or in groundwater artificial medium in light blue (23 spots). The Se(-II, -I) group includes organic Se compounds. See methods and Supporting Information for further details. Results of least-square linear combination fitting of all sample μXANES spectra are summarized in **Table S3**. Both analyses indicate that Se^0 is the main product in field-derived and culture samples.

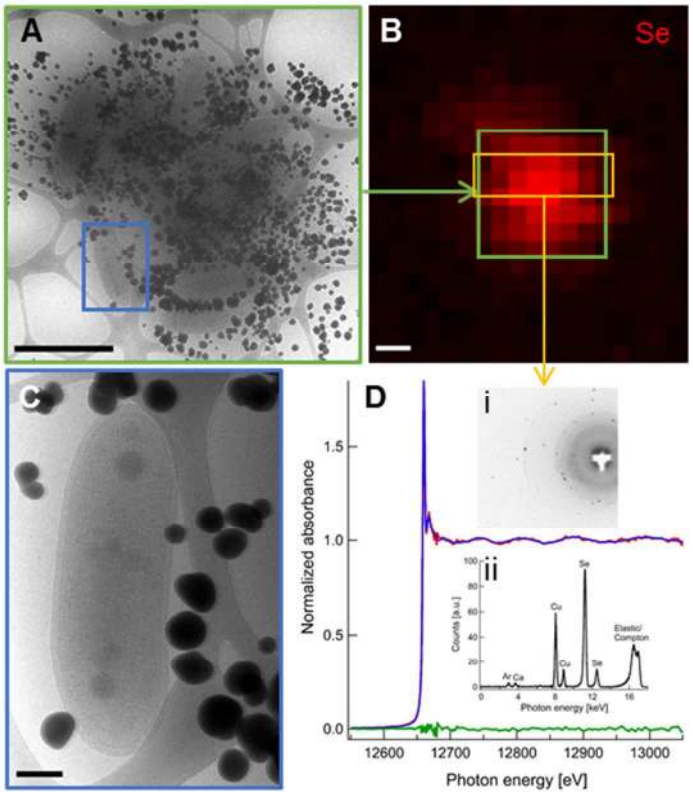

Figure 5. Correlative cryogenic spectro-microscopy on a 19-day-old culture grown in bicarbonate medium. A) Low dose cryo-TEM image (3.5 nm pixels, 7.2 x 7.2 μm^2) of a cluster of bacteria and associated Se CNP aggregates. B) Cryo-µXRF Se distribution map at 13keV (2 µm beam, 1 µm pixels). The green box area represents the entire TEM region. C) Low dose cryo-TEM image at higher magnification of the blue box area of panel A. D) Cryogenic Se K-edge µXANES (in red) collected in the orange box area of panel B. Best fit (in blue) is obtained using 87% red amorphous Se and 13% sodium selenite standards. Residual is plotted in green (normalized sum-sq is 1.25 10^{-4}). Insets i and ii: Cryo-µXRD pattern and -µXRF spectrum, respectively, collected at 17 keV in the orange box area. XRD showed no evidence for crystalline Se^0 (see **Figure S11)**. Red amorphous Se^0 aggregates (~ 100 ± 60 nm) is the main

product of selenate reduction in this region of the sample, with minor presence of Se(IV), suggesting a 2-step reduction process. Scale bars are 2 μm (A-B) and 200 nm (C).

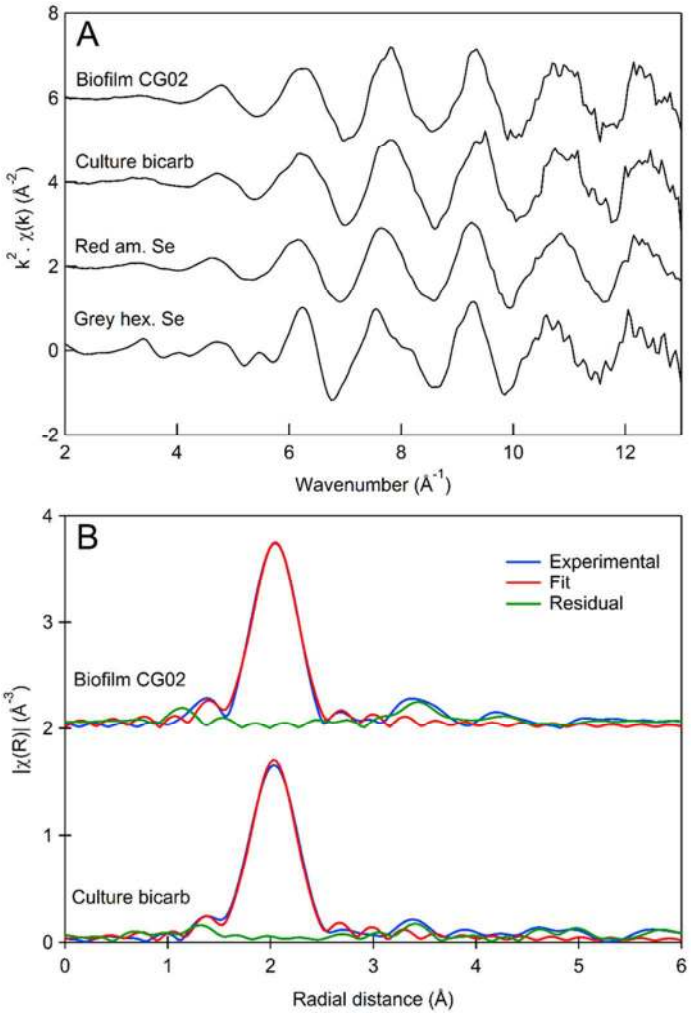

Figure 6. Cryo-μEXAFS of biofilm CG02 and of a 19-day-old selenate-reducing enrichment culture grown in bicarbonate medium A) in k-space, compared to red amorphous Se^0 and hexagonal grey Se^0 (Se foil) standards. B) Shell-by-shell fitting analysis of the 1st shell (**see Table S4**) with Se-Se interatomic distance at 2.355 ± 0.003 Å for the biofilm CG02 and 2.339 ± 0.003 Å for the culture. Experimental spectra are shown in blue, the fits (performed in q space) in red and the residuals in green.

TOC